Redox Biology 55 (2022) 102409

Contents lists available at ScienceDirect

Redox Biology

journal homepage: www.elsevier.com/locate/redox

Vanadium pentoxide induced oxidative stress and cellular senescence in human lung fibroblasts

Xiaojia He, Zachery R. Jarrell, Yongliang Liang, Matthew Ryan Smith, Michael L. Orr, Lucian Marts, Young-Mi Go *, Dean P. Jones **

Division of Pulmonary, Allergy and Critical Care Medicine, Emory University, Atlanta, GA, 30322, USA

ARTICLE INFO

Keywords:
Environmental health
Lung fibrosis
Redox cycling
Thiol/disulfide redox
Vanadate

ABSTRACT

Both environmental exposure to vanadium pentoxide (V_2O_5, V^{+5} for its ionic counterparts) and fibroblast senescence are associated with pulmonary fibrosis, but whether V^{+5} causes fibroblast senescence remains unknown. We found in a dose-response study that 2–40 μM V^{+5} caused human lung fibroblasts (HLF) senescence with increased senescence-associated β-galactosidase activity and p16 expression, while cell death occurred at higher concentration (LC_{50}, 82 μM V^{+5}). Notably, measures of reactive oxygen species (ROS) production with fluorescence probes showed no association of ROS with V^{+5}-dependent senescence. Preloading catalase (polyethylene-conjugated), a H_2O_2 scavenger, did not alleviate the cellular senescence induced by V^{+5}. Analyses of the cellular glutathione (GSH) system showed that V^{+5} oxidized GSH, increased GSH biosynthesis, stimulated cellular GSH efflux and increased protein S-glutathionylation, and addition of N-acetyl cysteine inhibited V^{+5}-elevated p16 expression, suggesting that thiol oxidation mediates V^{+5}-caused senescence. Moreover, strong correlations between GSSG/GSH redox potential (E_h), protein S-glutathionylation, and cellular senescence ($R^2 > 0.99$, $p < 0.05$) were present in V^{+5}-treated cells. Studies with cell-free and enzyme-free solutions showed that V^{+5} directly oxidized GSH with formation of V^{+4} and GSSG in the absence of O_2. Analyses of V^{+5} and V^{+4} in HLF and culture media showed that V^{+5} was reduced to V^{+4} in cells and that a stable V^{+4}/V^{+5} ratio was rapidly achieved in extracellular media, indicating ongoing release of V^{+4} and reoxidation to V^{+5}. Together, the results show that V^{+5}-dependent fibroblast senescence is associated with a cellular/extracellular redox cycling mechanism involving the GSH system and occurring under conditions that do not cause cell death. These results establish a mechanism by which environmental vanadium from food, dietary supplements or drinking water, can cause or contribute to lung fibrosis in the absence of high-level occupational exposures and cytotoxic cell death.

1. Introduction

Vanadium is a redox-active metal with relatively high abundance in the Earth's crust and variable content in human foods and drinking water [1]. Vanadium pentoxide (V_2O_5, V^{+5} for vanadate unless otherwise noted) in occupational and environmental exposures can cause respiratory distress, organ damage, or even death [1–8]. A large number of V^{+5} studies in rodents, primates and humans show impairment of lung function, increased pulmonary reactivity, histological alterations, bronchial lymph node hyperplasia, inflammation, and eventually lung fibrosis [9–15]. In contrast, a different oxidation state of vanadium, vanadyl sulfate ($VOSO_4$, V^{+4} for vanadyl unless otherwise noted) is widely consumed in dietary supplements for glucose regulation [16]. While the routes of exposure differ, V^{+4} is readily oxidized to V^{+5} under aerobic conditions [17], raising the possibility that V^{+5}, either from environmental exposure or derived from V^{+4} in dietary supplements, could be an insidious cause or contributor to fibrosing lung diseases, including idiopathic pulmonary fibrosis (IPF).

Increasing evidence indicates that fibroblast senescence can be important in the initiation and progression of pulmonary fibrosis [18–28]. Cellular senescence, a permanent cell cycle arrest without cell death, can be triggered or promoted by several mechanisms including the pro-inflammatory secretome in addition to unrepairable cellular damage [19,29–31]. Expression of cellular senescence markers in IPF lungs is closely associated with disease severity [23], and senescent fibroblasts are observed in IPF lungs and in fibroblast cultures from IPF lungs, providing a key pathological feature that is also evident in

* Corresponding author. Whitehead Biomedical Research Building, 615 Michael St, Room 225, Atlanta, GA, 30322, USA.
** Corresponding author. Whitehead Biomedical Research Building, 615 Michael St, Room 205P, Atlanta, GA, 30322, USA.
E-mail addresses: ygo@emory.edu (Y.-M. Go), dpjones@emory.edu (D.P. Jones).

https://doi.org/10.1016/j.redox.2022.102409
Received 2 May 2022; Received in revised form 30 June 2022; Accepted 12 July 2022
Available online 16 July 2022

Abbreviations:

BSA	bovine serum albumin
Cys	cysteine
CySS	cystine
CySSG	glutathione-cysteine disulfide
DCF	dichlorofluorescein
DCF-H_2	dichlorodihydrofluorescein
DCFH_2-DA	2′,7′ –dichlorofluorescein diacetate
DTNB	5,5′-dithio-bis-(2-nitrobenzoic acid
DTT	dithiothreitol
EDTA	Ethylenediaminetetraacetic acid
FBS	fetal bovine serum
Glc Ox	glucose oxidase
γ-Glu-Glu	γ-glutamylglutamate
GSH	glutathione
GSSG	glutathione disulfide
HBSS	Hank's balanced salt solution
HLF	human fetal lung fibroblasts
HPLC	high-performance liquid chromatography
IPF	idiopathic pulmonary fibrosis
NAC	N-acetyl cysteine
PBS	phosphate-buffered saline
PCA	perchloric acid
PEG-Cat	polyethylene glycol-conjugated catalase
PMSF	phenylmethylsulfonyl fluoride
PrSSG	protein S-glutathionylation
ROS	reactive oxygen species
SA-βgal	senescence-associated β-galactosidase
SOD	superoxide dismutase
TCA	trichloroacetic acid
TNB	2-nitro-5-thiobenzoic acid

experimental lung fibrosis models [23,25,27,28,32]. These lines of evidence point to the possibility that V^{+5}, even at concentrations which do not cause cell death, could cause or contribute to lung fibrosis.

Multiple oxidative mechanisms have been implicated in V^{+5}-dependent cell death, but the contribution of these mechanisms to cellular senescence in the absence of cell death is not known. One of these mechanisms involves generation of reactive oxygen species (ROS), including peroxovanadate complex with V^{+5} or peroxovanadyl complex with V^{+4}, with consequent macromolecular damage [33–47]. An alternative mechanism involves direct oxidation of GSH or protein thiols due to the strong oxidation potential by V^{+5}/V^{+4} [48–52]. In the present research, we performed dose-response studies with V^{+5} in human fetal lung fibroblasts (HLF) and found that V^{+5} caused cellular senescence at concentrations that did not promote cell death. Systematic evaluation of mitochondrial and cellular ROS, cellular GSH and protein S-glutathionylation showed that V^{+5}-dependent fibroblast senescence correlated with GSH oxidation and protein S-glutathionylation, but not H_2O_2 or ROS signals. Results showed that V^{+5} directly oxidized GSH by a mechanism which was independent of O_2 and not blocked by catalase, which catalyzes the reduction of H_2O_2. Added catalase blocked H_2O_2 accumulation but did not block protein S-glutathionylation or HLF senescence. These results establish a mechanism by which V^{+5} contributes to fibroblast senescence. Because fibroblast senescence is associated with the development of pulmonary fibrosis, the results suggest that environmental V^{+5} may contribute to fibrosis without evident cell death or tissue injury.

2. Materials and methods

2.1. Chemicals

Vanadium pentoxide (V_2O_5), catalase-polyethylene glycol (PEG-Cat, ~40,000 units/mg protein), glucose oxidase (Glc Ox, Type VII, ≥100,000 units/g solid from *Aspergillus niger*), dithiothreitol, trichloroacetic acid, perchloric acid, sodium iodoacetate, KOH, potassium tetraborate, dansyl chloride, methanol, doxorubicin, butyrate, H_2O_2, bovine serum albumin (BSA), EDTA, tetrabutyl ammonium, and ammonium hydroxide were purchased from Sigma-Aldrich (St. Louis, MO). Triton® X-100 was purchased from Promega Corporation (Madison, WI). H_3PO_4 was purchased from Acros Organics (Belgium). Dithiothreitol (DTT) was purchased from Bio-Rad (Canada). Boric acid was purchased from J.T.Baker™ (Phillipsburg, NJ). γ-Glutamylglutamate (γ-Glu-Glu) was purchased from MP Biomedical, Inc. (Solon, OH). All reagents were analytical grade or above unless otherwise stated.

2.2. Cell culture

Human fetal lung fibroblasts (HLF) were obtained from American Tissue Culture Collection (passages 6-9, ATCC, Rockville, MD). HLF were cultured using F-12K medium (Kaighn's Modification of Ham's F-12 medium) with 10% fetal bovine serum (FBS) and 100 U/mL penicillin/streptomycin, and maintained in a humidified incubator at 5% CO_2 and 37 °C. Culture medium with low FBS (0.5%) was used for continued cell culture at the time of treatment.

2.3. Cytotoxicity assay

The WST-1 assay used to determine cytotoxicity is based on the conversion of the tetrazolium salt (WST-1) to a formazan via the succinate-tetrazolium reductase activity, which is active only in living cells. HLF were counted (Countess® II FL Automated Cell Counter, Life Technologies Corporation, Bothell, WA) and 5×10^4 cells/well were seeded overnight in a 96-well plate with 8 replicates for each treatment. The cells were then treated with different concentrations of V^{+5} (0-400 μM, corresponding to 0-200 μM V_2O_5.) for 24 h. Following the incubation periods, the WST-1 assay was performed by adding 20 μL of WST reagents (Roche) to each well (200 μL cell culture media), and HLF were further incubated at 37 °C for 4 h. After incubation, the absorbance of the cells was measured at 450 nm relative to a reference wavelength at 610 nm using an ELISA platereader (SpectraMax M2).

2.4. Senescence assay

Senescence-associated β-galactosidase (SA-βgal) activity of HLF cells was determined using chromogenic methods according to manufacturer's instruction (Cell Signaling Technology, Inc., Danvers, MA). In brief, cells were fixed with 2% formaldehyde and 0.2% glutaraldehyde for 15 min at room temperature after removing media and rinsing once with PBS. Fixed cells were then incubated overnight at 37 °C in a dry incubator (without CO_2) in a freshly prepared staining solution at pH 6.0 consisting of 1 mg/mL 5-bromo-4-chloro-3-indolyl β-D-galactopyranoside (X-Gal). To stain the nuclei, fixed cells were washed in PBS, and then stained with Hoechst 33342 1:2500 (trihydrochloride, trihydrate, Invitrogen) at 5% CO_2 and 37 °C for 5 min. Cells were kept in 70% glycerin after removing staining solution. β-galactosidase activity was imaged with brightfield microscopy (BioTek Lionheart FX, Winooski, VT) at 10× magnification, cell nuclei stained with Hoechst 33342 were imaged with fluorescent microscopy at excitation and emission wavelengths of 350 and 461 nm, respectively. Cellular senescence was calculated by manually enumerating blue stained cells indicating β-galactosidase activity relative to the total cell number based upon

nuclei count. Nine images with at least 100 cells were captured from each well with at least 3 replicates. In addition, protein expression of p16 (cyclin-dependent kinase inhibitor 2A) for a mediator of cell senescence was examined by Western blot analysis (see below).

2.5. Cell membrane permeability and DNA damage assay

Cells were seeded into 96-well plate and incubated at 5% CO_2 and 37 °C for 24 h to reach 80% confluence. Cell membrane permeability and DNA damage were measured using the HCS DNA Damage Kit (Invitrogen, USA) following the procedure provided by manufacturer. In brief, at the end of V^{+5} or other chemical exposure, 50 μL Image-iT® DEAD Green™ viability solution was added into each well that contains 100 μL incubation medium for 30 min under normal cell culture conditions. Cells were then fixed with 4% methanol-free paraformaldehyde solution, and permeabilized with 0.25% Triton® X-100, for 15 min each. After blocking with 1% BSA in PBS cells were probed with 50 μL (1:1000) phosphorylated H2AX (Ser139) mouse monoclonal antibody, and 50 μL (1:2000) Alexa Fluor® 555 goat anti-mouse IgG (H + L) mixed with Hoechst 33342 (1:6000), for 60 min each. After washing with PBS, the fluorescence intensities for each staining were analyzed with a fluorescence plate reader (SpectraMax M2). Butyrate (5 μM, 24h), doxorubicin (1 μM, 2h) and H_2O_2 (2 mM, 2h) were used as positive controls.

2.6. Intracellular reactive oxygen species (ROS)

We use ROS to collectively describe reactive oxidants produced in response V^{+5} treatment, including but not limited to H_2O_2, peroxynitrite, and superoxide anion radical. The intracellular formation of ROS was detected using the probe 2′,7' –dichlorofluorescein diacetate ($DCFH_2$-DA) (Invitrogen) [53]. $DCFH_2$-DA is a cell-permeable, non-fluorescent dye that, once inside the cell, is hydrolyzed by intracellular esterase to non-fluorescent dichlorodihydrofluorescein (DCF-H_2). The latter reacts with intracellular oxidants to form the highly fluorescent product dichlorofluorescein (DCF), the fluorescence intensity of which is proportional to ROS production. Control experiments showed that $DCFH_2$-DA does not directly react with V^{+5}. In brief, cells at >80% confluency were treated with V^{+5} for 24 h and loaded with $DCFH_2$-DA (100 μM) in 96-well plate and incubated with 5% CO_2 at 37 °C for 30 min. Fluorescence was measured using fluorescence plate reader (SpectraMax M2, Molecular Devices, Sunnyvale, CA) with excitation at 485 nm and emission at 530 nm.

2.7. Mitochondrial ROS production

All procedures were performed at 5% CO_2 at 37 °C. HLF were incubated for 48 h in 96-well plates started at 1×10^3 cells/well. Cell medium was removed and cells were treated with vanadium for 1 h. After vanadium treatment, the medium was removed and cells were washed 3 times with pre-warmed HBSS (hanks balanced salt solution. 100 μL MitoTracker® Red CM-H_2XRos (200 nM in HBSS) was added to each well and incubated for 30 min. Each well was then aspirated to remove medium and washed 3 times with pre-warmed HBSS. 100 μL MitoSOX™ Red (5 μM in HBSS w/Ca/Mg) was added to each well and incubated for 15 min. All cell media were removed and washed 3 times with pre-warmed HBSS and added 200 μL pre-warmed F-12K media. The cell-permeant MitoTracker® Red CM-H2XRos probes contain a mildly thiol-reactive chloromethyl moiety for labeling mitochondria. The fluorescence intensity of MitoTracker® Red CM-H2XRos was measured with a fluorescence plate reader at excitation and emission wavelengths of 579 and 599 nm, respectively. MitoSOX™ Red mitochondrial superoxide indicator is a fluorogenic dye for detection of superoxide in the mitochondria of live cells and was measured with a fluorescence plate reader at excitation and emission wavelengths of 579 and 599 nm, respectively. Cells treated with 2 mM H_2O_2 were used as positive control.

2.8. Western blotting

Western blot analysis was employed to examine protein levels of catalase in HLF cells preloaded with PEG-Cat. Cells were incubated at the indicated conditions, harvested, and lysed using cell lysis Pierce® RIPA buffer containing protease inhibitor (cOmplete™, Mini, EDTA-free Protease Inhibitor Cocktail, Roche) and 1 mM PMSF. 20 μg of protein was used for Western blot analysis to prove with the primary antibodies specific for catalase, β-actin or p16 (Cell Signaling Technology, Inc.) and proteins were visualized as previously described [54,55].

2.9. GSH redox measurement

HLF after V^{+5} treatment were analyzed using a fluorescence assay for GSH, GSSG, glutathione-cysteine disulfide (CySSG), cysteine (Cys) and cystine (CySS) using high-performance liquid chromatography (HPLC) with a gradient HPLC module 2695 (Waters), a multi λ fluorescence detector 2475 (Waters) at excitation wavelength of 335 nm and emission wavelength of 518 nm and Empower software using SUPELCOSIL™ LC-NH_2 HPLC Column (25 cm × 4.6 mm, 5 μm) as previously described [56]. Briefly, 175 μL cell culture media was removed from 6-well plates and added to an equal volume of 10% PCA containing 0.2 M boric acid and 10 μM γ-Glu-Glu. For cellular redox measurement, cells were rinsed twice with ice cold PBS and collected in 375 μL ice cold 5% PCA containing 0.2 M boric acid and 10 μM γ-Glu-Glu internal standard. Both cells and media were centrifuged at 14,000×*g*, 4 °C for 2 min. 300 μL of the supernatant were then transferred to new tubes and 60 μL of 50 mM sodium iodoacetate were added at room temperature. pH was adjusted to 9 using KOH-TB (1 M KOH with 0.38 M potassium tetraborate) and incubated at room temperature for 20 min. 300 μL of 75 mM dansyl chloride were added, and all tubes were left in the dark overnight. Finally, 500 μL of chloroform were added into the solution. Extracted solutions were vortexed and centrifuged at 14,000×*g*, 4 °C for 2 min. 50 μL of top clear solution were injected and concentrations of GSH, GSSG, and CySSG were calculated relative to the internal standard γ-Glu-Glu and normalized to the protein concentration. The individual concentrations, expressed in molar values, were used with the Nernst equation to calculate redox potentials for GSH/GSSG (E_hGSSG/GSH) with E_o = −240 mV, pH 7.0. Cell pellets were collected and dissolved in 200 μL 1 M NaOH and 5 μL of the dissolved cell pellets were used for protein assay using Pierce BCA assay.

2.10. Protein S-glutathionylation

Protein S-glutathionylation was quantified by measuring protein-bound GSH relative to total protein concentration as previously described [57]. Briefly, media was removed, and cells were washed twice with phosphate-buffered saline (PBS). Cell lysates were collected in 200 μL 10% trichloroacetic acid (TCA) and centrifuged at 16,800×*g* for 5 min, at 4 °C. Cell pellets were then washed in 25% TCA. After removing supernatant by centrifuging at 16,800×*g* for 5 min at 4 °C, cell proteins were resolubilized in 200 μL 1 M NaOH. 125 μL of protein solution were mixed 1:1 with 5 mM DTT in 0.1 M sodium phosphate buffer (pH 6) and incubated for 30 min at room temperature. Reduced protein was reprecipitated by mixing samples 1:1 with 10% PCA containing 0.2 M boric acid and 10 μM γ-Glu-Glu internal standard. GSH released from protein was quantified by HPLC with fluorescence detection (Waters 2695), as described above. 5 μL solubilized protein was analyzed for protein concentration using the Pierce BCA protein assay.

2.11. V-GSH kinetics assay

V^{+5}, V^{+4}, and GSSG were quantitatively determined using HPLC (Waters 2690) with UV–vis detector at 240 nm (Waters 2487). The

mobile phase for isocratic elution was composed of 4% MeOH, 18 mM EDTA, 0.5 mM tetrabutyl ammonium, 20 mM H_3PO_4, with pH adjusted to 7 with concentrated ammonium hydroxide (NH_4OH). A flow rate of 1 mL/min was used with a C_{18} column (Ascentis, 15 cm × 4.6 mm, 5 μm). The retention time for GSSG was 2.4 min, V^{+4} was 3.4 min, and V^{+5} was 6 min. Concentrations of V^{+5}, V^{+4} and GSSG were calculated against standard curves (Supplemental Fig. S1).

2.12. Ellman's assay

Total thiols were determined using Ellman's reagent, 5,5′-dithio-bis-(2-nitrobenzoic acid (DTNB), that reacts with thiol groups and produces yellow-colored 2-nitro-5-thiobenzoic acid (TNB). Briefly, 20 μL sample was mixed with 75 μL dilution buffer (30 mM Tris HCl, 3 mM EDTA, pH 8.2), 25 μL DTNB (3 mM in MeOH), and 400 μL MeOH. Mixed samples were centrifuged, and total thiol content was calculated from absorbance at 412 nm against standard curve using GSH as reference.

2.13. BCA protein assay

Protein concentration was measured in 5 μL of cell samples using Pierce™ BCA Protein Kit (Thermo Scientific) in a 96-well plate reader. After addition of 200 μL of working reagent to each well, mixing and incubation for 30 min, absorbance was measured at 562 nm (SpectraMax M2, Molecular Devices).

2.14. Statistical analysis

Data from at least three independent replicates of each experimental condition were compared using one-way ANOVA followed by Fisher's Least Significant Difference (LSD) post-hoc tests. Two-way ANOVA analysis followed by Fisher's LSD post-hoc tests was used to investigate the multiple variant comparisons for the time and dose effects, with $p < 0.05$ considered significant. Pearson's correlation coefficient R and adjusted R^2 were calculated for linear regression. Data were represented as mean ± standard error of the mean (SEM).

3. Results

3.1. V^{+5} increases HLF cell senescence without cell death

To determine V^{+5} cytotoxicity in HLF, we measured cell death following V^{+5} concentrations ranging from zero to 400 μM. The analyses showed that 50% (LC_{50}) and 80% cell death occurred at 82 μM and 100 μM V^{+5} treatment, respectively (Fig. 1A). No apparent cell death was observed with V^{+5} concentrations lower than 40 μM (<10% death, Fig. 1B). Quantification of cellular vanadium by ICP-MS confirmed HLF uptake at 2, 20 and 40 μM treatment of V^{+5} (Supplemental Fig. S2). At concentrations below 1 μM, vanadium uptake could not be detected due to instrument sensitivity for detection with the cell culture conditions used.

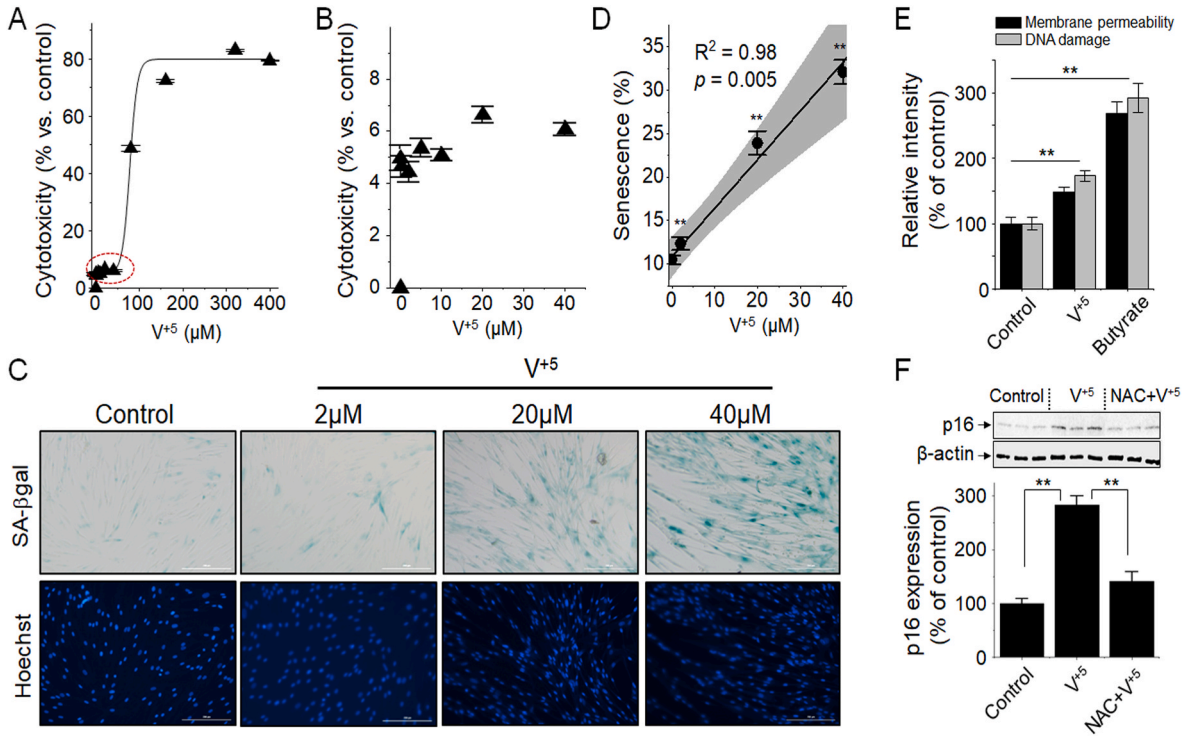

Fig. 1. Vanadium pentoxide (V^{+5})-dependent cytotoxicity and cellular senescence in human lung fibroblasts (HLF). A) Cytotoxicity towards HLF induced by V^{+5} exposure was quantified using WST1 assay after 24 h. Vanadium pentoxide produces 2 vanadate ions in solution and data are provided in terms of vanadate concentration. **B)** Minimal cytotoxicity occurred at 40 μM V^{+5} and lower concentrations (expanded from red circle in Panel A). **C)** Cellular senescence caused by V^{+5} exposure was determined by measuring SA-βgal activity (left panels) by microscopy at 24 h. Cell nuclei were stained by Hoechst 33342 dye (right) for cell number quantification. **D)** Quantitative and statistical analysis of cellular senescence induced by V^{+5} at various concentrations. **E)** Cells treated with 40 μM V^{+5} show increased cell membrane permeability (Image-iT® DEAD Green™ viability stain) and DNA damage (phosphorylated H2AX level). Butyrate (5 μM) was used as a positive control. Fluorescence intensities were normalized to cell number measured by Hoechst 33342 dye. **F)** Expression of p16 protein as a mediator of cellular senescence was examined by Western blotting (top, n = 3). Quantitative and statistical analysis of p16 expression, relative to β-actin, in response to V^{+5} at 40 μM, with or without pretreatment of N-acetyl cysteine (NAC, 5 mM) overnight are presented by a bar graph. Nine images, with at least 100 cells per image, were captured from each well, and each condition had at least 3 biological replicates. Data are shown as mean ± SEM. Statistical significance for each condition vs. control, or between conditions is indicated by asterisks, with $^{**}p < 0.01$.*P*values were determined by two-way ANOVA followed by LSD post-hoc with n = 8 for cytotoxicity assay, n = 13–16 for DNA damage assay, and n = 3 for senescence and western blotting assay. Grey shading indicates 95% confidence interval. (For interpretation of the references to color in this figure legend, the reader is referred to the Web version of this article.)

To examine whether V^{+5} exposure caused HLF cellular senescence, cells were exposed to increasing doses of V^{+5} (2, 20, and 40 μM) for 24 h and the biomarker of senescence [58], senescence-associated β-galactosidase (SA-βgal) was measured as a measure of cellular senescence. More SA-βgal-stained cells were observed at 2 μM (12.4 ± 2.1%) in comparison to control (10.3 ± 0.5%), and were greater at 20 μM (26.8 ± 2.1%) and 40 μM (45.7 ± 4.2%) of V^{+5} (Fig. 1C and D). Cell nuclei staining by Hoechst dye confirmed similar cell densities for different treatment groups (Fig. 1C). Additionally, correlation analysis showed that the SA-βgal staining increased with V^{+5} concentration over the range of 2–40 μM V^{+5} (Fig. 1D). To examine whether V^{+5} causes cell senescence by involving DNA damage, we measured DNA double-strand break and cell membrane permeability. Elevated phosphorylation of the histone variant H2AX (Ser-139) to form γH2AX is an early cellular response to DNA double-strand breaks [59]. Therefore, phosphorylated H2AX is recognized as the second most common marker of cellular senescence in addition to SA-βgal [60]. As shown in Fig. 1E, our data indicate that the phosphorylated H2AX level was higher after treating the cells with 40 μM V+5 (172.7 ± 8.3%, $p < 0.01$) than in the control cells. Butyrate (5 μM, 24h), doxorubicin (1 μM, 2h) and H_2O_2 (2 mM, 2h) were used as positive controls, showing substantially high phosphorylated H2AX levels with 291.9 ± 21.8% ($p < 10^{-10}$), 509.9 ± 30.3% ($p < 10^{-10}$), and 514.3 ± 60.2% ($p < 10^{-10}$) increases comparing to controls, respectively. Moreover, expression of p16 (cyclin-dependent kinase inhibitor 2A) as a marker of cell senescence was significantly increased by V^{+5} exposure at 40 μM (Fig. 1F, $p < 0.001$), and the pretreatment of N-acetyl cysteine (NAC) overnight diminished p16 expression by V^{+5} (Fig. 1F, $p < 0.01$). Taken together, the results of SA-βgal staining, DNA damage measurement and elevation of p16 indicate that V^{+5} increases cellular senescence in HLF under conditions that cause little to no cell death.

3.2. V^{+5}-associated HLF senescence is independent of ROS generation

Previous research shows that reactive oxygen species (ROS) can stimulate cellular senescence [61–63]. Therefore, we used fluorescent indicators of ROS production to test whether V^{+5}-dependent SA-βgal staining is associated with increased ROS production. In these experiments, we restricted studies to 2–40 μM V^{+5} concentrations because this range had measurable increase in SA-βgal staining with little to no cell death. To quantify cellular ROS production, we used the non-specific ROS cell probe, $DCFH_2$-DA (Fig. 2A and B), which accumulates in cells as a fluorescent product upon oxidation. Quantification of cellular DCF fluorescence showed a 2-fold increase in oxidant production in response to 2 μM V^{+5} but no apparent dose-dependence (2–40 μM) in ROS formation (Fig. 2B). Results with a mitochondria-targeted, non-specific ROS indicator, MitoTracker® Red CM-H2XRos, showed a similar increase in ROS by approximately 1.9-fold without an apparent dose response from 2 to 40 μM V^{+5} (Fig. 2C). Similarly, measurement of effects of 2–40 μM V^{+5} on MitoSOX™ Red, a selective indicator of mitochondrial $O_2^{\bullet-}$ production, showed 1.5-fold increase in oxidant production with no apparent dose-response effect (Fig. 2D).

Because V^{+5} showed a dose-response effect on SA-βgal activity, but did not show a dose-dependent effect on ROS production, we used glucose oxidase (Glc Ox)-dependent generation of H_2O_2 production to test for H_2O_2-dependent increase in HLF senescence. We first verified H_2O_2 production (Fig. 3A) and cell loading with the H_2O_2-metabolizing enzyme catalase (Cat), delivered as polyethylene glycol (PEG)-conjugated Cat (1000 U/mL) (Fig. 3B), in which endogenous cellular Cat was used as a loading control. With this defined system we found that 100 mU/mL Glc Ox caused H_2O_2 production and increased SA-βgal staining (Fig. 3C–E). Under these conditions, treatment with PEG-Cat (1000 U/mL) decreased Glc Ox-increased ROS and SA-βgal staining, thereby confirming that increased H_2O_2 induces cellular senescence in HLF and that this H_2O_2-dependent cellular senescence is blocked by a treatment that decreased cellular H_2O_2.

Based upon this evidence that PEG-Cat at 1000 U/mL blocked SA-βgal staining caused by oxidant production at a level comparable to that caused by 40 μM V^{+5} (Fig. 3C), we used this concentration of PEG-Cat to test whether H_2O_2 plays a role in V^{+5}-dependent senescence. The results showed that PEG-Cat did not prevent SA-βgal staining caused by V^{+5} exposure (Fig. 3D). This direct comparison (Fig. 3D and E), along with the lack of V^{+5} dose-response effect on oxidant levels in HLF (Fig. 2), indicates that cellular senescence following V^{+5} exposure occurs by a mechanism that is independent of increased cellular ROS generation.

3.3. V^{+5} stimulates oxidation of glutathione (GSH) and cellular release of GSH

GSH oxidation, protein S-glutathionylation, and the resulting lung redox imbalance, are associated with cellular senescence [64–66] and IPF [67,68]. V^{+5} can directly oxidize thiols [49], raising the possibility

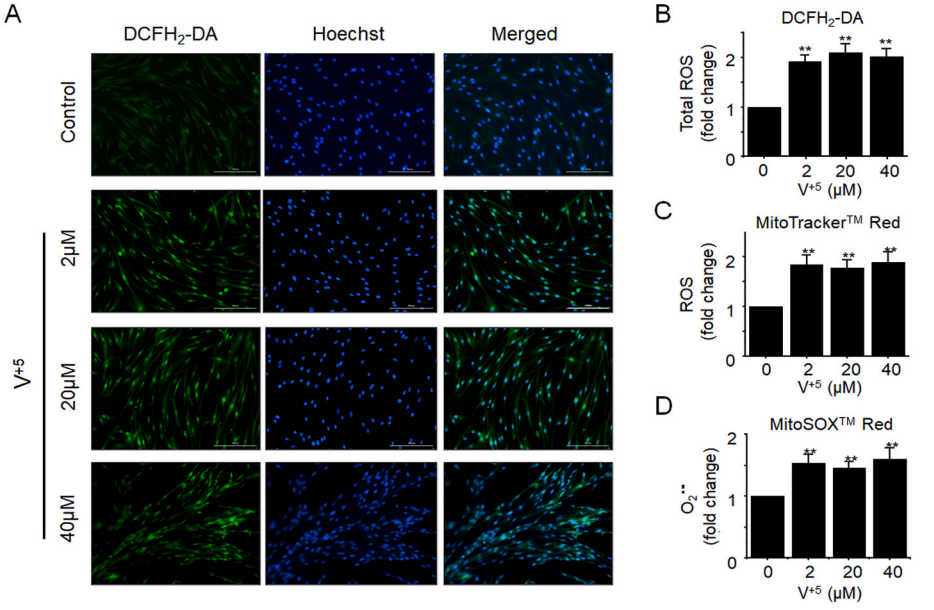

Fig. 2. Vanadium pentoxide (V^{+5})-dependent ROS production in HLF. A) Representative images from $DCFH_2$-DA treated cells (left) show increase in total cellular ROS production induced by V^{+5} exposure. Cell nuclei were stained by Hoechst (middle panels). Merged images (right) show correspondence of fluorescein staining with cell nuclei staining. **B)** Measurement of total ROS production as in panel A using a fluorescence plate reader (excitation at 485 nm and emission at 530 nm). **C)** Measurement of mitochondrial ROS using MitoTracker™ Red (excitation at 579 and emission at 599 nm). **D)** Measurement of mitochondrial superoxide production using MitoSOX™ Red as a fluorescence indicator (excitation at 579 and emission at 599 nm). Results shown in Panels B, C and D are mean ± SEM for 8 wells per treatment and representative of at least 3 biological replicates. Statistical comparisons were obtained by one-way ANOVA followed by LSD post-hoc with n = 8, with comparisons shown relative to control, $^{**}p < 0.01$. (For interpretation of the references to color in this figure legend, the reader is referred to the Web version of this article.)

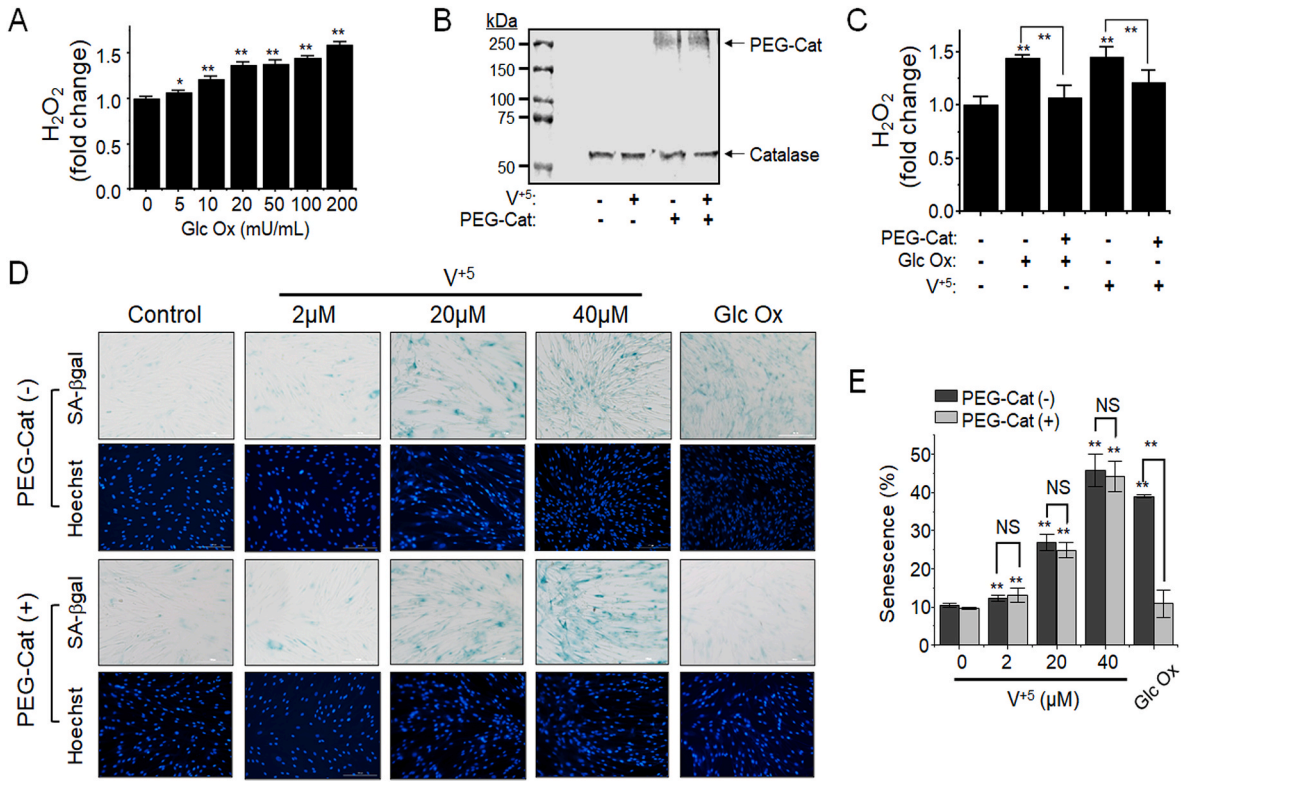

Fig. 3. Vanadium pentoxide (V^{+5})-induced senescence in HLF was independent of ROS production. **A)** A test system for H_2O_2-dependent senescence was established using $DCFH_2$-DA assay to measure ROS production at 6 h after addition of extracellular Glc Ox. **B)** A test system for H_2O_2-dependent senescence was established using Western blot showing cellular PEG-Cat (~250 kDa) abundance in HLF cells 24 h after added PEG-Cat (1000 U/mL). Endogenous catalase (~60 kDa) is also evident in the Western blot. **C)** Results from $DCFH_2$-DA assay showing that PEG-Cat (1000 U/mL) decreased H_2O_2 detection following Glc Ox (100 mU/mL) for 6 h or V^{+5} (40 μM) for 24 h. **D)** Cell images showing that PEG-Cat does not prevent V^{+5}-dependent senescence as measured by SA-βgal activity while it inhibits Glc Ox-elevated cell senescence. **E)** Quantification of results as in Panel D using cell counts to test the hypothesis that decreased H_2O_2 by treatment with PEG-Cat blocks senescence as measured by SA-βgal. 1000 U/mL PEG-Cat and 50 mU/mL Glc Ox were used for studies in Panels B–E. Data are shown as mean ± SEM for 8 wells per treatment and representative of at least 3 biological replicates. Statistical comparisons were obtained by one-way ANOVA followed by LSD post-hoc with n = 8, with comparisons shown relative to control, with $*p < 0.05$ and $**p < 0.01$. NS, not significant.

that V^{+5} could cause oxidative stress and induce cellular senescence by direct effects on the cellular GSH system without ROS as an intermediate. Additionally, inhibition of V^{+5}-elevated p16 by NAC (Fig. 1E) led us to examine the effects of V^{+5} on the GSH system over the same V^{+5} concentration range as used for SA-βgal staining and ROS production. Assays for GSH, GSSG and cysteine-glutathione disulfide (CySSG) showed a complex pattern of responses, indicating 1) oxidation of GSH, 2) stimulation of GSH biosynthesis, and 3) stimulation of cellular efflux of GSH, GSSG and CySSG in response to V^{+5}-dependent oxidative stress (Fig. 4). Cellular GSH showed an apparent biphasic response with an increase at 40 μM and a non-significant decrease at 2 and 20 μM (Fig. 4A). At 2 and 20 μM, there was no significant increase in measured cellular GSSG, but GSSG was increased at 40 μM (Fig. 4B). However, cellular CySSG was increased at each concentration (Fig. 4C), and the steady-state cellular GSH/GSSG redox potential (E_h) was more positive at each concentration (Fig. 4D). Because the data for 40 μM V^{+5} are consistent in showing oxidation of cellular GSH system, i.e., increased GSSG (Fig. 4B), increased CySSG (Fig. 4C), more positive E_h (Fig. 4D), and the increased GSH (Fig. 4A) demonstrates oxidative stress-induced GSH biosynthesis [69], the most consistent interpretation of the cumulative data is that V^{+5} causes an oxidation of the cellular GSH system at all concentrations over the range of 2–40 μM V^{+5}. This is supported by calculation of the GSH/GSSG ratio, which decreased from 125 to 52 following exposure to 40 μM V^{+5}. A similar trend in cysteine/cystine redox cycle was also observed in HLF cells exposed to V^{+5} (Supplemental Fig. S3), further suggesting altered cellular redox environment by exposing to V^{+5}. As shown above, preloading NAC, a potent antioxidant against protein thiol oxidation [70] and precursor for GSH biosynthesis [71] decreased the cellular senescence induced by V^{+5} exposure (Fig. 1E), indicating that GSH oxidation stimulated by V^{+5} played a central role in the observed cellular senescence (Fig. 1C and D).

Examination of culture media showed that extracellular levels of GSH (Fig. 4E), GSSG (Fig. 4F) and CySSG (Fig. 4G) were all increased as a function of V^{+5} concentration, demonstrating increased export of GSH species. Because extracellular GSH is known to interact with the extracellular cysteine/cystine pool in culture media, these results do not provide information about which of the forms of GSH are exported. However, a biphasic effect on extracellular E_h for the GSH/GSSG pool, with a more negative (reduced) value at 2 μM V^{+5} with increased contribution from additional factors (stimulated efflux of GSSG and/or CySSG; stimulated oxidation of GSH or other thiols by oxidation, e.g., by V^{+5}) at 20 and 40 μM V^{+5}. To examine the apparent stimulation of GSH release in more detail, we examined the time-course of release with 40 μM V^{+5}. Two-way ANOVA showed increased extracellular GSH (Fig. 5A) and GSSG (Fig. 5B) for the V^{+5}-treated groups ($p < 0.01$), incubation time ($p < 0.01$), and V^{+5} treatment × incubation time ($p < 0.01$), with a relatively constant extracellular GSH/GSSG ratio (~0.76). The relatively constant extracellular GSH/GSSG over time indicates that the extracellular GSH system could be responding to both changes in cellular release of GSH species and with 1-electron oxidation-reduction reactions, such as those involved in oxidation-reduction of V^{+5} and V^{+4} (see below).

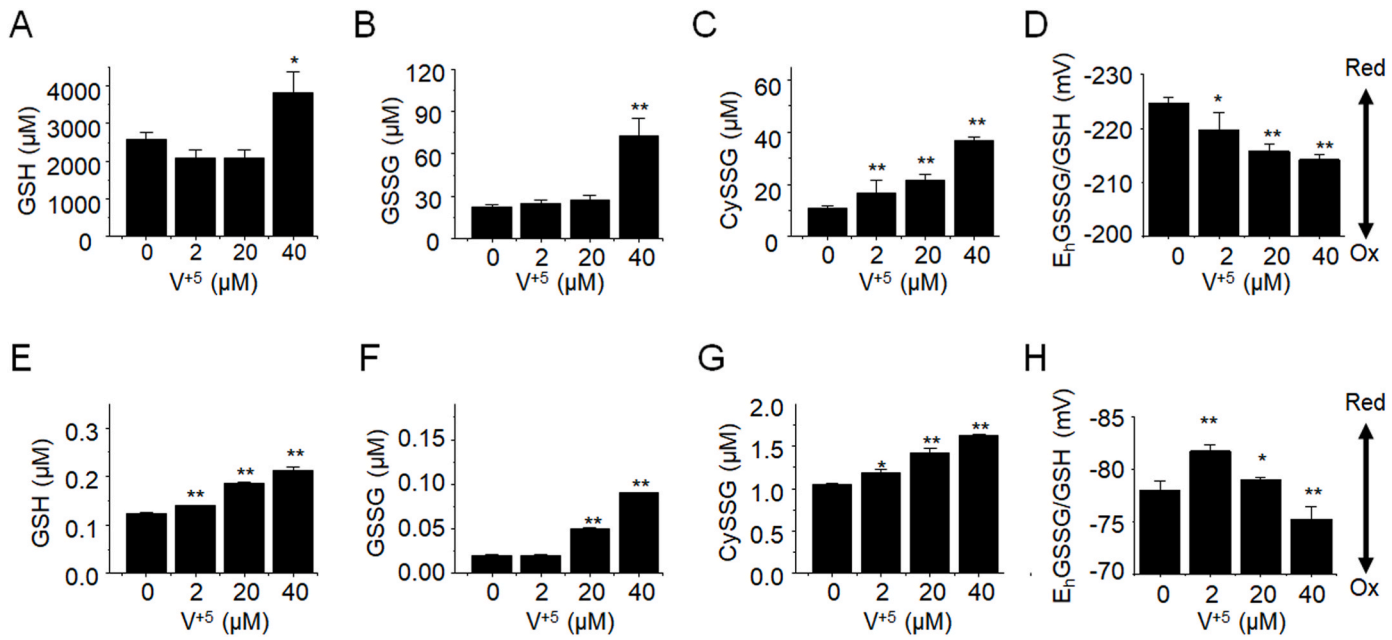

Fig. 4. Senescence-inducing V^{+5} concentrations cause complex responses of HLF cellular and extracellular GSH system. A)-D): Cellular response of GSH redox system to V^{+5}. **A)** Biphasic dose-response effect shows increase in cellular GSH. **B)** Monotonic increase in cellular GSSG with V^{+5} shows concentration-dependent GSH oxidation. **C)** Monotonic increase in cellular Cys-GSH disulfide (CySSG) with V^{+5} provides evidence for concentration-dependent increase in GSH synthesis and oxidation of the cellular GSH pool. **D)** Calculated steady-state cellular GSSG/GSH redox potential (E_hGSSG/GSH) shows oxidation with increasing V^{+5} concentration. **E)-H):** Extracellular response of GSH redox system to V^{+5}. **E)** Increase in extracellular GSH as a function of V^{+5} concentration provides evidence for stimulated GSH synthesis and export. **F)** Increase in extracellular GSSG as a function of V^{+5} concentration provides evidence for GSH oxidation and stimulated GSSG export. **G)** Increase in extracellular CySSG as a function of V^{+5} concentration and increased cellular CySSG provides evidence for stimulated CySSG export. **H)** Biphasic change in extracellular E_hGSSG/GSH with increasing V^{+5} shows that minimal cellular oxidative stress at low V^{+5} stimulates GSH synthesis and export while higher concentrations cause more extensive oxidative stress and more extensive export of disulfide forms. Data are shown as mean ± SEM. Statistical significance for each condition vs. control is indicated by asterisks, with $*p < 0.05$ and $**p < 0.01$. P values were determined by one-way ANOVA followed by LSD post-hoc with n = 12 to 24 per group.

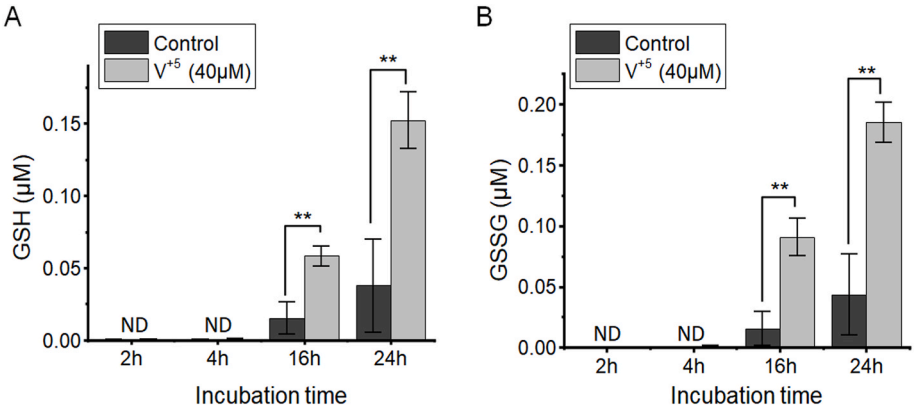

Fig. 5. Senescence-inducing V^{+5} concentration addition to HLF causes time-dependent increase in GSH and GSSG in culture medium. A) Time course of change in GSH concentration in culture media following addition of 40 μM V^{+5}. **B)** Time course of change in GSSG concentration in culture media following addition of 40 μM V^{+5}. Results show that both GSH and GSSG are increased in the extracellular culture medium with a ratio of GSH/GSSG that is largely preserved despite evidence for increased oxidative stress. Data are shown as mean ± SEM. Statistical significance for each condition vs. control, or between conditions is indicated by asterisks, with $**p < 0.01$. P values were determined by two-way ANOVA followed by LSD post-hoc with n = 3. ND, not detected.

3.4. V^{+5}-dependent increased protein S-glutathionylation contributes to cell senescence

Protein S-glutathionylation (PrSSG) is an important mechanism for regulation of protein activities and commonly increases when the ratio of GSH/GSSG decreases [72,73]. As shown in Fig. 6, PrSSG was increased at all tested V^{+5} concentrations ($p < 0.01$). A strong dose-response relationship was present in HLF exposed to V^{+5} ($R^2 = 0.94$; $p < 0.05$, Supplemental Fig. S4), with 3-fold increase in PrSSG at 40 μM V^{+5} in comparison to control ($p < 0.01$, Fig. 6A). Moreover, PrSSG is significantly associated with cellular V^{+5} uptake ($R^2 = 0.84$, $p < 0.05$, Supplemental Fig. S5A) and cell senescence ($R^2 = 0.89$, $p < 0.05$, Supplemental Fig. S5C). In contrast, no apparent relationship existed between PrSSG and either of the measures of ROS (Supplemental Figs. S6A–C). To test for contribution of H_2O_2 produced from V^{+5} exposure to PrSSG, we preloaded HLF cells with PEG-Cat (1000 U/mL) and employed Glc Ox (100 mU/mL) as a positive control. PrSSG due to Glc Ox treatment was blocked by preloading PEG-Cat (1000 U/mL). In contrast, preloading PEG-Cat did not prevent the rise in PrSSG induced by V^{+5} exposure (Fig. 6B). These results support the interpretation that at levels associated with HLF senescence, V^{+5} increases PrSSG by a ROS-independent mechanism.

3.5. Direct thiol oxidation by V^{+5}

Because V^{+5} is an oxidant and our data show that V^{+5}-dependent

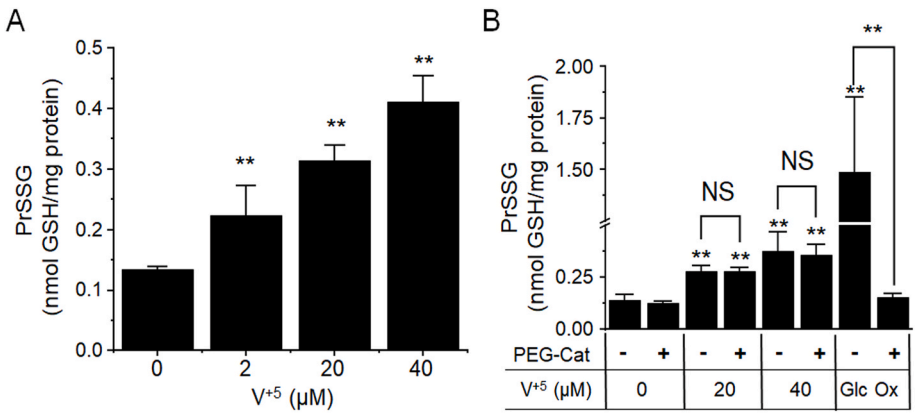

Fig. 6. Protein S-glutathionylation (PrSSG) of HLF is increased following exposure to senescence-causing V^{+5} exposure by a process that is not blocked by catalase. A) Cellular PrSSG was measured at 24 h after addition of V^{+5} at concentrations indicated. Total protein-GSH disulfide was measured as GSH released following reduction with DTT and expressed relative to measured cellular protein. **B)** Experiments with PEG-Cat (1000 U/mL) showed that catalase at a concentration that removed H_2O_2 generated by Glc Ox (100 mU/mL) (see Fig. 3) prevented PrSSG by Glc Ox but did not block PrSSG due to 20 or 40 μM V^{+5}. Cells with V^{+5} were incubated for 24 h, and experiments with Glc Ox were incubated for 6 h. Data were shown as mean ± SEM. Statistical significance is given relative to control and indicated by asterisks, with $^{**}p < 0.01$. P values were determined by one-way ANOVA followed by LSD post-hoc with n = 3. NS, not significant.

PrSSG formation in HLF is largely H_2O_2-independent, we performed experiments to determine whether GSH, the major low-molecular weight thiol in cells, is directly oxidized by V^{+5}. GSSG (Δ) was formed from GSH by reaction with 40 μM vanadium pentoxide in solution without added cells or enzymes (Fig. 7A). Concurrent reduction of V^{+5} to V^{+4} was measured by HPLC, and the reaction approached completion within 120 min. In expression of the stoichiometry, V_2O_5 produces two V^{+5} ions per molecule, and 2 GSH are consumed per GSSG formed. Thus, when expressed in common 1-electron transfer forms, the results show that GSSG (Δ) was formed from GSH as expected from the reduction of vanadate (V^{+5}, ●), to vanadyl ions (V^{+4}, ■) (Fig. 7A). The main V^{+5} ion present in the physiological condition is $VO_2(OH)_2^-$; whereas, at acidic pH, the main ion is VO_2^+. Our primary goal was to illustrate the reduction from V^{+5} to V^{+4} in cells and in the presence of GSH without cells; therefore, we assumed $VO_2(OH)_2^-$ and VO^{2+} were the main V^{+5} and V^{+4} species, respectively, under our experimental conditions [74]. An alternative assay for total thiol loss independently confirmed the GSH loss in response to V^{+5} addition (Fig. 7B). To test for the possibility that H_2O_2 was an intermediate in the reaction due to vanadium-dependent catalysis of GSH reaction with O_2 in solution, we added PEG-Cat (1000U/mL) to the reaction and found no effect on enzyme-free oxidation of GSH by V^{+5} (Fig. 7C). To further test for O_2 dependence of the reactions, we repeated the experiment using solutions that were de-gassed and purged overnight with ultrapure N_2 in order to remove O_2, and found no difference in rates (data not shown).

To obtain additional information on the reaction rates, we performed experiments with varied V^{+5} concentrations. Assuming that GSH oxidation was a second order reaction [75], the possible reactions involved in the direct oxidation of GSH by V^{+5} are:

$$V_2O_5(s) + 3H_2O(aq) \rightarrow 2VO_2(OH)_2^-(aq) + 2H^+(aq) \quad (1)$$

$$VO_2(OH)_2^-(aq) + GSH(aq) + 3H^+(aq) \rightarrow VO^{2+}(aq) + GS^{\cdot}(aq) + 3H_2O(aq) \quad (2)$$

$$2GS^{\cdot}(aq) \rightarrow GSSG(aq) \quad (3)$$

The exact vanadium species present in the solution and biological systems are rather complicated due to the coordination sphere of vanadium in water, and this varies with the oxidation state and environmental pH [74]. We describe the rate of V^{+5} reduction as

$$R_{(2)} = k\left[VO_2(OH)_2^-\right][GSH] \quad (4)$$

where k is the rate constant ($M^{-1}\ s^{-1}$), and initial $VO_2(OH)_2^-$ was 40 μM and GSH was 5 mM. We use the production of V^{+4} as $R_{(2)}$ to estimate the rate constant k. Using the measured initial rate of V^{+4} production, $\partial V^{+4}/\partial t = 0.4$ μM min^{-1} and Equation (1), we obtain an estimate for the second order rate constant $k = 0.03\ M^{-1}\ s^{-1}$. Notably, this should be considered an estimate because a slower initial reaction rate might occur due to rate of formation of an intermediate V^{+5}-thiol complex as a pre-equilibrium step before reduction [49].

In light of these data showing direct oxidation of GSH by V^{+5}, the high cellular GSH concentration, and the low extracellular GSH and GSSG, we further examined the oxidation state of vanadium in cells and

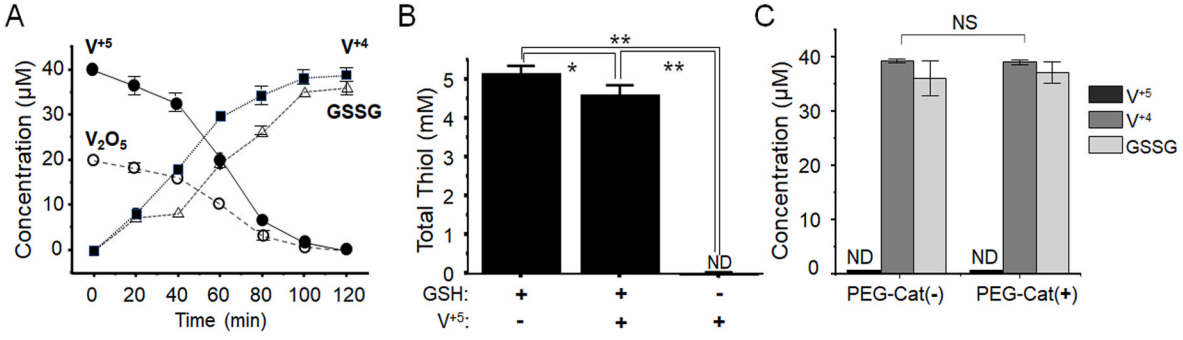

Fig. 7. Direct oxidation of GSH by reaction with V^{+5} occurs in cell-free system. A) Addition of 40 μM V^{+5} to 5 mM GSH-containing solution (pH 7, 37 °C) resulted in loss of V^{+5} (vanadate ions, filled circles), and appearance of V^{+4} (squares) and GSSG (triangles) as determined by HPLC. GSSG is expressed in molar equivalents of GSH for the 1-electron reaction to illustrate stoichiometry of the reaction. Data for V^{+5} expressed as vanadium pentoxide added is shown as open circles. **B)** HPLC assay with UV/Vis detection as used in Panel A did not detect GSH so data in this panel show results for thiol measurement using Ellman's assay. Results for GSH at 2 h showed GSH loss as predicted from the reaction stoichiometry. **C)** Inclusion of catalase (1000U/mL) did not change the oxidation of GSH by V^{+5} without enzymes. Data were shown as mean ± SEM. Statistical significance for each condition vs. control is indicated by asterisks, with $^{*}p < 0.05$ and $^{**}p < 0.01$. P values were determined by one-way ANOVA followed by LSD post-hoc with n = 3. NS, not significant. ND, not detected.

culture medium after addition of V^{+5}. HPLC analyses of HLF showed that after V^{+5} addition, V^{+4} was present in cells but V^{+5} was undetectable (Fig. 8A). In contrast, both V^{+4} and V^{+5} were measurable in extracellular media and, after an hour, were maintained at a relatively stable V^{+5}/V^{+4} ratio of 1.2–1.25 during the remaining 24-h culture period (Fig. 8B). To examine the potential reaction between V^{+5}/V^{+4} and culture media, we recorded the V^{+4} and V^{+5} concentrations over 2 h in culture medium without cells. There was no accumulation of V^{+4} in media (without cells) containing V^{+5} at physiological pH (Fig. 8C). Because V^{+4} can re-oxidize back to V^{+5} at pH 7, we adjusted the cell media to pH in order to inhibit reoxidation and quantify the potential reduction of V^{+5} caused by the media. As shown in Fig. 8C, approximately 10% of the added V^{+5} was reduced to V^{+4} by media after 1 h of incubation and increased to 20% at 2 h of incubation. In contrast, analysis of V^{+4} oxidation by culture medium at pH 7 showed that 94% of added V^{+4} was oxidized to V^{+5} in 1 h. These data show that even though components in the media can reduce V^{+5} in the absence of cells, oxidation of V^{+4} to V^{+5} occurred at a much faster rate (Fig. 8D). Thus, the evidence shows that the relatively stable V^{+5}/V^{+4} ratio observed in culture media in the presence of cells (Fig. 8B) occurs with ongoing oxidation-reduction processes involving both cellular and extracellular reactions of the V^{+5}/V^{+4} and disulfide/thiol systems.

4. Discussion

The present study shows that vanadate (V^{+5}), a relatively abundant, ionic form of a redox-active transition metal known to be associated with pulmonary fibrosis due to occupational exposures [10,12], induces cellular senescence in human lung fibroblasts (HLF) at non-cytotoxic concentrations. This finding accentuates health concerns of exposure to vanadium compounds because cellular senescence can initiate fibrosis and contribute to fibrosing lung diseases, including IPF [18–28]. Environmental vanadium is highly variable in food and drinking water, and vanadium-containing dietary supplement use is unregulated. Consequently, transient exposure to vanadium compounds that cause lung fibroblast senescence could contribute to increased incidence of idiopathic fibrotic lung disease.

The present studies provide evidence for a mechanism of vanadium-induced senescence which could ultimately yield new biomarkers to assess risk for development and progression of fibrotic lung disease. The data suggest that a vanadium redox cycle exists in which V^{+5} is reduced to V^{+4} in cells, oxidizing GSH, stimulating GSH synthesis and increasing export of GSH species. Because V^{+4} is oxidized to V^{+5} by O_2 and other oxidants [17], cellular release of V^{+4} and GSH species with oxidation of V^{+4} back to V^{+5} creates a redox cycle which places an oxidative stress burden on cells as long as vanadium is present. This mechanism does not exclude contribution of ROS to vanadium-dependent toxicities, but provides evidence that direct oxidation of the GSH system by V^{+5} is sufficient to cause fibroblast cell senescence as an activating step without invoking a ROS-dependent mechanism.

This interpretation is important because the cytotoxic effect of V^{+5} has previously been attributed to ROS production [33–37]. V^{+5}-induced ROS was proposed to be dependent on the mitochondria electron transport chain in which one electron is donated to O_2 leading to superoxide ($O_2^{\bullet-}$) formation and resultant reduction of V^{+5} [in form of $VO_2(OH_2)^-$] to V^{+4} [in form of VO^{2+}], as depicted in Reactions (4-6). The generated $O_2^{\bullet-}$ is transformed to H_2O_2 by superoxide dismutase (SOD), which can be decomposed by catalase, as shown in Reactions (7-8).

$$NADPH \rightarrow NADP^{+} + H^{+} + 2e^{-},\ E^{\circ'} = -0.324V \quad (5)$$

$$VO_2(OH)_2^{-}(aq) + e^{-} + 4H^{+} \rightarrow VO^{2+} + 3H_2O,\ E^{\circ'} = 0.58V \quad (6)$$

$$O_2 + e^{-} \rightarrow O_2^{\bullet-},\ E^{\circ'} = -0.16V \quad (7)$$

$$2O_2^{\bullet-} + 2H^{+} \xrightarrow{SOD} H_2O_2 + O_2 \quad (8)$$

$$2H_2O_2 \xrightarrow{catalase} 2H_2O + O_2 \quad (9)$$

H_2O_2 generated from Reaction (7) has been speculated as the main cause for the V^{+5}-induced oxidative stress [33–37]. Furthermore, H_2O_2 is well-known for promoting oxidative stress-induced premature senescence [63]. We confirmed that H_2O_2 produced by Glc Ox leads to significant PrSSG and cellular senescence and that preloading HLF with PEG-Cat prevented these responses. In contrast, our results with V^{+5} showed that preloading PEG-Cat in HLF prevented intracellular H_2O_2 accumulation but did not prevent the PrSSG nor cellular senescence. This is corroborated by a study from Cortizo et al. (2000) who also found

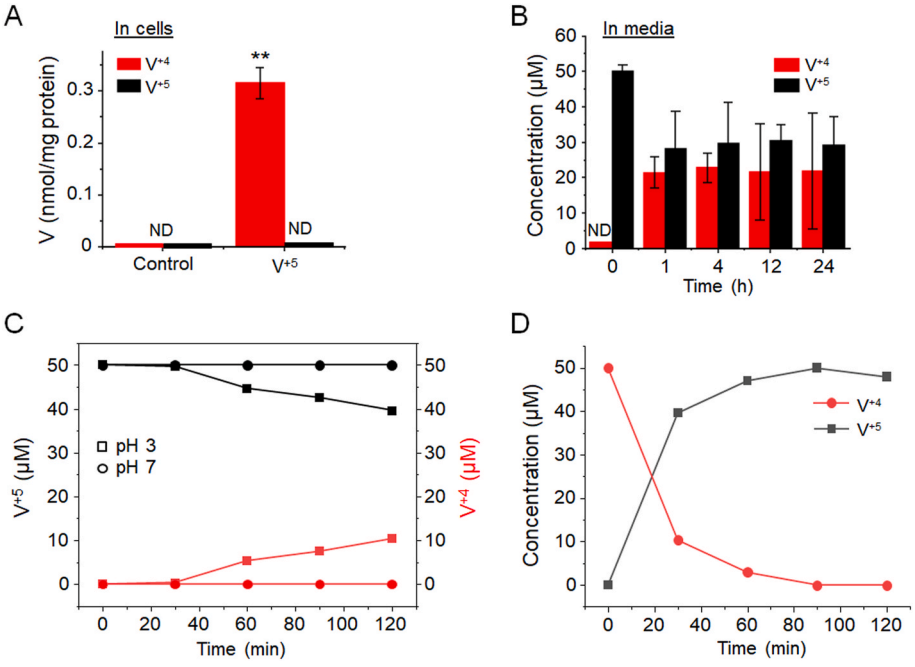

Fig. 8. Stable extracellular V^{+5}/V^{+4} ratio is rapidly achieved in HLF cell culture with senescence-inducing V^{+5} concentrations. A) Measured V^{+4} and V^{+5} by HPLC shows only V^{+4} is detectable at 24 h. **B)** Time course of concentrations of V^{+4} and V^{+5} in culture medium after addition of 50 μM V^{+5} shows stable extracellular V^{+5}/V^{+4} ratio is rapidly achieved. **C)** Addition of 50 μM V^{+5} to culture medium at pH 7.0 without cells shows no detectable loss of V^{+5} (black circles) or appearance of V^{+4} (red circles); whereas, with culture media at pH 3 where O_2-dependent oxidation of V^{+4} does not occur, a slow rate of reduction of V^{+5} is observed (black squares) with appearance of V^{+4} (red squares). **D)** Addition of 50 μM V^{+4} to culture medium at pH 7.0 without cells shows rapid oxidation of V^{+4} (red) to V^{+5} (black). Data were shown as mean ± SEM or as representative data from at least 3 experiments. Statistical significance for each condition vs. control is indicated by asterisks, with $^{**}p < 0.01$. P values were determined by one-way ANOVA followed by LSD post-hoc with n = 3. ND, not detected. (For interpretation of the references to color in this figure legend, the reader is referred to the Web version of this article.)

that eliminating ROS production did not improve the V^{+5}-dependent cytotoxicity [76]. Similarly, Zhang et al. found that supplementing antioxidants [superoxide dismutase (SOD), formate, and catalase] to cells treated with 100 μM V^{+5} did not fully recover cells from V^{+5}-induced cell growth arrest at the G2/M phase [77]. In their study, growth arrest was about 10% in control cells and 30% in V^{+5}-treated cells. Catalase inhibited V^{+5}-induced H_2O_2 formation by 70%, and decreased cell growth arrest from about 30% to 20%. Neither a superoxide scavenger SOD nor a hydroxyl radical scavenger formate, exhibited any effect on cell growth arrest. Thus, a large portion of high-dose V^{+5}-induced cell growth arrest at the G2/M phase could be attributed to other factors, such as direct thiol oxidation by V^{+5}. The decoupling between ROS production and V^{+5} cytotoxicity was also proposed by Capella et al. (2007) in four different cell lines including K562, K562-Lucena 1, MDCK, and Ma104 [78]. Other research shows that V^{+5} can form peroxovanadate complex with H_2O_2 [33–47], and diperoxovanadate can induce premature senescence [79]. While PEG-Cat can be expected to decrease formation of peroxovanadate complex [80], additional research is needed to clarify the relative contribution of a peroxovanadate mechanism to the V^{+5}-dependent HLF senescence.

Our research corroborates previous studies indicating that V^{+5} oxidizes GSH and protein thiols [48–52], in addition to V^{+5} to V^{+4} conversion intracellularly [50,51] as well as directly by reaction with GSH [49]. For example, studies using ^{48}V tracer showed that GSH reduced orthovanadate (VO_4^{3-}) to V^{+4} in human red blood cells [50]. Our estimate for the reaction rate constant for GSH and V^{+5} (0.03 M^{-1} s^{-1}) is approximately 10-fold slower than reaction rate constant (0.42 M^{-1} s^{-1}) for GSH oxidation by H_2O_2 [81], and 4-fold higher than reaction rate constant (0.008 M^{-1} s^{-1}) for GSH oxidation by nitric oxide [82]. These comparisons indicate that reaction of GSH with V^{+5} occur at rates that are comparable to physiologically important reactivities.

Impaired GSH redox homeostasis has been well-documented in mouse models of fibrosis [68,83], and is thought to be an important mediator of pulmonary fibrosis and reduced lung function in humans [84–86]. A review by Liu and Pravia outlines how disrupted GSH redox status and increased oxidative stress are closely associated with TGF-β mediated pulmonary fibrosis [86]. Moreover, changes in the cellular GSH redox state may cause disrupted cellular signaling [87–90] and premature senescence [65]. Characterizing GSH redox status therefore may provide a valuable means to detect vanadium-dependent redox cycling in order to mitigate cellular senescence and subsequent pulmonary fibrosis. Finally, the interplay and potential synergistic effects of aberrant GSH redox status attributed to vanadium exposure coupled with pre-existing risk factors for pulmonary fibroblast senescence and pulmonary fibrosis such as telomere-related genetic mutations have yet to be evaluated and warrant further exploration [91].

The present study further suggest that PrSSG may provide a useful pathway for biomarker development in regards to development and progression of pulmonary fibrosis. PrSSG is considered as a defense mechanism to protect proteins from oxidative stress via a reversible modification of thiol groups controlled by glutaredoxins (Grx) [92]. Increasing PrSSG indicates a regulated cellular response to oxidative stress (Fig. 6), which is in agreement with changes in cellular GSH/GSSG and E_hGSSG/GSH. Earlier studies reported that Grx activity was substantially decreased in fibrotic lungs, while PrSSG was significantly increased [93]. Similarly, PrSSG levels were significantly increased in lungs of mice with oxidant-induced acute lung injury and pulmonary fibrosis [94]. It has also been noted that reducing protein oxidation could potentially reverse lung fibrosis [93].

There are several limitations to this study. Multiple biologic processes contribute to cellular senescence, and the etiology of fibrosing lung diseases, including IPF, is multifactorial such that vanadium may have a small contribution to total disease burden. Additionally, the GSH system and inducibility of the system declines with age. Thus, vanadium-dependent effects mediated through the GSH system may be amplified or diminished by age-associated changes, and additional studies are necessary to examine the impact of aging on V^{+5}-dependent cellular senescence. Finally, lungs are complex structures with localized cellular environments, multiple cell types, and specialized subcellular compartments. Thus, the current model of V^{+5}/V^{+4} redox cycling between cellular and extracellular compartments will require additional refinement to better understand mechanistic details.

5. Conclusions

The present results show that sublethal V^{+5} exposure causes a dose-response effect on the cellular and extracellular GSH antioxidant system, PrSSG and cellular senescence in HLF cells without dependence upon ROS intermediates. Results showed that GSH was oxidized by V^{+5} without enzymes or requirement for O_2 or ROS intermediate. Cellular senescence due to V^{+5} exposure was attributed to the high oxidizing potential of V^{+5}, which caused elevated GSSG/GSH ratio, more positive E_h GSSG/GSH value, stimulated GSH species export and increased PrSSG. Analyses of V^{+5} and V^{+4} showed a stable extracellular V^{+5}/V^{+4} ratio over time, indicating that cellular-extracellular redox cycling of V^{+5} and V^{+4} could result in sustained cellular oxidative stress causing DNA damage and cell cycle arrest as long as vanadium is present in the biological system. Further studies are needed to understand compartmental effects, mechanistic details and time-dependent responses which could impact the role of V^{+5} in the pathogenesis of lung fibrosis.

Author contributions

X.H., Y.M.G., and D.P.J. contributed to conceptualization, methodology, and writing. X.H. contributed to sample processing, data curation and formal analysis. Z.R.J., Y.L., M.R.S., M.L.O., and L.M. contributed to sample processing and methodology. Y.M.G. and D.P.J. contributed to supervision, funding acquisition, and project administration.

Funding

This study was supported by National Institute of Environmental Health Sciences grants R21 ES031824 (DPJ and YMG), R01 ES031480 (YMG), R01 ES023485 (DPJ and YMG), P30 ES019776 (DPJ), R01 ES032189 (DPJ), F32 ES033908 (ZJ) and T32 ES012870 (ZJ), and National Institute of Diabetes Digestive and Kidney Disease grant RC2 DK118619 (DPJ) and R01 DK125246 (YMG, DPJ).

Declaration of competing interest

The authors declare no competing financial interests.

Acknowledgments

Drs. Young-Mi Go and Dean P. Jones share equal senior authorship in this collaborative research.

Appendix A. Supplementary data

Supplementary data to this article can be found online at https://doi.org/10.1016/j.redox.2022.102409.

References

[1] ATSDR, Toxicological Profile for Vanadium, U.S. Department of Health & Human Services. Agency for Toxic Substances and Disease Registry, 2012.
[2] R. Hauser, et al., A prospective study of lung function among boilermaker construction workers exposed to combustion particulates, Am. J. Ind. Med. 39 (2001) 454–462.
[3] J.L. Domingo, Vanadium: a review of the reproductive and developmental toxicity, Reprod. Toxicol. 10 (3) (1996) 175–182.
[4] F.L. Assem, L.S. Levy, A review of current toxicological concerns on vanadium pentoxide and other vanadium compounds: gaps in knowledge and directions for future research, J. Toxicol. Environ. Health, Part A B 12 (4) (2009) 289–306.

[5] J. Yang, et al., Leaching characteristics of vanadium in mine tailings and soils near a vanadium titanomagnetite mining site, J. Hazard Mater. 264 (2014) 498–504.
[6] T.I. Fortoul, et al., Overview of environmental and occupational vanadium exposure and associated health outcomes: an article based on a presentation at the 8th International Symposium on Vanadium Chemistry, Biological Chemistry, and Toxicology, Washington DC, August 15–18, 2012, J. Immunot. 11 (1) (2014) 13–18.
[7] V.A. Ehrlich, et al., Inhalative exposure to vanadium pentoxide causes DNA damage in workers: results of a multiple end point study, Environ. Health Perspect. 116 (12) (2008) 1689–1693.
[8] F.L. Assem, L.S. Levy, in: Vanadium, H. Michibata (Eds.), Chapter 10. Inhalation Toxicity of Vanadium, Springer, Dordrecht, 2012, pp. 9–224.
[9] E.A. Knecht, et al., Pulmonary reactivity to vanadium pentoxide following subchronic inhalation exposure in a non-human primate animal model, J. Appl. Toxicol. 12 (6) (1992) 427–434.
[10] National Toxicology Program, NTP toxicology and carcinogensis studies of vanadium pentoxide (CAS No. 1314-62-1) in F344/N rats and B6C3F1 mice (inhalation), Natl. Toxicol. Progr. Tech. Rep. 507 (2002) 1–343.
[11] E.A. Knecht, et al., Pulmonary effects of acute vanadium pentoxide inhalation in monkeys, Am. Rev. Respir. Dis. 132 (6) (1985) 1181–1185.
[12] J.C. Bonner, et al., Airway fibrosis in rats induced by vanadium pentoxide, Am. J. Physiol. Lung Cell Mol. Physiol. 278 (1) (2000) L209–L216.
[13] E.A. Rondini, D.M. Walters, A.K. Bauer, Vanadium pentoxide induces pulmonary inflammation and tumor promotion in a strain-dependent manner, Part. Fibre Toxicol. 7 (2010) 9.
[14] R. Hauser, et al., Spirometric abnormalities associated with chronic bronchitis, asthma, and airway hyperresponsiveness among boilermaker construction workers, Chest 121 (2002) 2052–2060.
[15] G.B. Irsigler, P.J. Visser, P.A. Spangenberg, Asthma and chemical bronchitis in vanadium plant workers, Am. J. Ind. Med. 35 (1999) 366–374.
[16] P. Poucheret, et al., Vanadium and diabetes, Mol. Cell. Biochem. 188 (1-2) (1998) 73–80.
[17] D.C. Crans, A.S. Tracey, The chemistry of vanadium in aqueous and nonaqueous solution, in: A.S. Tracey, D.C. Crans (Eds.), Vanadium Compounds: Chemistry, Biochemistry, and Therapeutic Applications, American Chemical Society, 1998, pp. 2–29.
[18] F. Hernandez-Gonzalez, et al., Cellular senescence in lung fibrosis, Int. J. Mol. Sci. 22 (13) (2021) 7012.
[19] R.-M. Liu, G. Liu, Cell senescence and fibrotic lung diseases, Exp. Gerontol. 132 (2020), 110836.
[20] M.J. Schafer, et al., Cellular senescence mediates fibrotic pulmonary disease, Nat. Commun. 8 (2017), 14532.
[21] T. Parimon, M.S. Hohmann, C. Yao, Cellular senescence: pathogenic mechanisms in lung fibrosis, Int. J. Mol. Sci. 22 (12) (2021) 6214.
[22] A. Venosa, Senescence in pulmonary fibrosis: between aging and exposure, Front. Med. 7 (2020), 606462.
[23] J.N. Justice, et al., Senolytics in idiopathic pulmonary fibrosis: results from a first-in-human, open-label, pilot study, EBioMedicine 40 (2019) 554–563.
[24] D.L. Kellogg 3rd, et al., Cellular senescence in idiopathic pulmonary fibrosis, Curr. Mol. Biol. Rep. 7 (2021) 31–40.
[25] D.W. Waters, et al., Fibroblast senescence in the pathology of idiopathic pulmonary fibrosis, Am. J. Physiol. Lung Cell Mol. Physiol. 315 (2) (2018) L162–L172.
[26] A.A. Mailleux, B. Crestani, Licence to kill senescent cells in idiopathic pulmonary fibrosis? Eur. Respir. J. 50 (2017), 1701360.
[27] D. Álvarez, et al., IPF lung fibroblasts have a senescent phenotype, Am. J. Physiol. Lung Cell Mol. Physiol. 313 (6) (2017) L1164–L1173.
[28] M.J. Schafer, et al., Cellular senescence mediates fibrotic pulmonary disease, Nat. Commun. 8 (1) (2017) 1–11.
[29] V. Gorgoulis, et al., Cellular senescence: defining a path forward, Cell 179 (2019) 813–827.
[30] R. Tacutu, et al., Molecular links between cellular senescence, longevity and age-related diseases - a systems biology perspective, Aging 3 (2011) 1178–1191.
[31] B.G. Childs, et al., Cellular senescence in aging and age-related disease: from mechanisms to therapy, Nat. Med. 21 (2015) 1424–1435.
[32] Y. Lin, Z. Xu, Fibroblast senescence in idiopathic pulmonary fibrosis, Front. Cell Dev. Biol. 8 (2020), 593283.
[33] M.M. De Cunha Padua, et al., Toxicity of native and Oxovanadium (IV/V) galactomannan complexes on HepG2 cells is related to impairment of mitochondrial functions, Carbohydr. Polym. 173 (2017) 665–675.
[34] G. Guerrero-Palomo, et al., Vanadium compounds and cellular death mechanisms in the A549 cell line: the relevance of the compound valence, J. Appl. Toxicol. 39 (3) (2018) 540–552.
[35] C. Fleury, B. Mignotte, J.-L. Vayssière, Mitochondrial reactive oxygen species in cell death signaling, Biochimie 84 (2-3) (2002) 131–141.
[36] L. Wang, et al., Vanadium-induced apoptosis and pulmonary inflammation in mice: role of reactive oxygen species, J. Cell. Physiol. 195 (2003) 99–107.
[37] M. Ding, et al., Vanadate-induced activation of activator protein-1: role of reactive oxygen species, Carcinogenesis 20 (4) (1999) 663–668.
[38] L.S. Capella, et al., Mechanisms of vanadate-induced cellular toxicity: role of cellular glutathione and NADPH, Arch. Biochem. Biophys. 406 (1) (2002) 65–72.
[39] A. Morinville, D. Maysinger, A. Shaver, From Vanadis to Atropos: vanadium compounds as pharmacological tools in cell death signalling, Trends Pharmacol. Sci. 19 (11) (1998) 452–460.
[40] S.J. Ruff, K. Chen, S. Cohen, Peroxovanadate induces tyrosine phosphorylation of multiple signaling proteins in mouse liver and kidney, J. Biol. Chem. 272 (2) (1997) 1263–1267.
[41] L.A. Scheving, J.R. Thomas, L. Zhang, Regulation of intestinal tyrosine phosphorylation and programmed cell death by peroxovanadate, Am. J. Physiol. Cell Physiol. 277 (3) (1999) C572–C579.
[42] S. Grillo, et al., Peroxovanadate induces tyrosine phosphorylation of phosphoinositide-dependent protein kinase-1 potential involvement of src kinase, Eur. J. Biochem. 267 (22) (2000) 6642–6649.
[43] R.K. Yamazaki, et al., The effects of peroxovanadate and peroxovanadyl on glucose metabolism in vivo and identification of signal transduction proteins involved in the mechanism of action in isolated soleus muscle, Mol. Cell. Biochem. 273 (1-2) (2005) 145–150.
[44] T.F. Cruz, A. Morgan, W. Min, In vitro and in vivo antineoplastic effects of orthovanadate, Mol. Cell. Biochem. 153 (1-2) (1995) 161–166.
[45] C. Hiort, J. Goodisman, J.C. Dabrowiak, Chemically and photochemically initiated DNA cleavage by an insulin-mimetic bisperoxovanadium complex, Cell. Biochem. Mol. 153 (1995) 31–36.
[46] C. Hiort, J. Goodisman, J.C. Dabrowiak, Cleavage of DNA by the insulin-mimetic compound, NH4[VO(O2)2(phen)], Biochemistry 35 (1996) 12354–12362.
[47] R. Faure, et al., Arrest at the G2/M transition of the cell cycle by protein-tyrosine phosphatase inhibition: studies on a neuronal and a glial cell line, J. Cell. Biochem. 58 (1995) 389–401.
[48] M. Mukhtiar, et al., Evaluation of the interaction of vanadium with glutathione in human blood components, Pak. J. Pharm. Sci. 25 (3) (2012) 549–553.
[49] W. Legrum, The mode of reduction of vanadate (+ V) to oxovanadium (+ IV) by glutathione and cysteine, Toxicology 42 (2-3) (1986) 281–289.
[50] I.G. Macara, K. Kustin, L.C. Cantley Jr., Glutathione reduces cytoplasmic vanadate mechanism and physiological implications, Biochim. Biophys. Acta 629 (1980) 95–106.
[51] L.C. Cantley Jr., P. Aisen, The fate of cytoplasmic vanadium. Implications on (NA, K)-ATPase inhibition, J. Biol. Chem. 254 (6) (1979) 1781–1784.
[52] X. Shi, N.S. Dalal, Flavoenzymes reduce vanadium(V) and molecular oxygen and generate hydroxyl radical, Arch. Biochem. Biophys. 289 (1991) 355–361.
[53] P.J. Halvey, et al., Selective oxidative stress in cell nuclei by nuclear-targeted D-amino acid oxidase, Antioxidants Redox Signal. 9 (7) (2007) 807–816.
[54] Y.M. Go, M. Orr, D.P. Jones, Increased nuclear thioredoxin-1 potentiates cadmium-induced cytotoxicity, Toxicol. Sci. 131 (1) (2013) 84–94.
[55] X. Hu, et al., Cadmium stimulates myofibroblast differentiation and mouse lung fibrosis, Toxicology 383 (2017) 50–56.
[56] D.P. Jones, Redox potential of GSH/GSSG couple: assay and biological significance, Methods Enzymol. 348 (2002) 93–112.
[57] Y.M. Go, et al., Selective protection of nuclear thioredoxin-1 and glutathione redox systems against oxidation during glucose and glutamine deficiency in human colonic epithelial cells, Free Radic. Biol. Med. 42 (2007) 363–370.
[58] F. Debacq-Chainiaux, et al., Protocols to detect senescence-associated beta-galactosidase (SA-βgal) activity, a biomarker of senescent cells in culture and in vivo, Nat. Protoc. 4 (12) (2009) 1798–1806.
[59] L.J. Mah, A. El-Osta, T.C. Karagiannis, γH2AX as a molecular marker of aging and disease, Epigenetics 5 (2) (2010) 129–136.
[60] A. Bernadotte, V.M. Mikhelson, I.M. Spivak, Markers of cellular senescence. Telomere shortening as a marker of cellular senescence, Aging 8 (1) (2016) 3–11.
[61] A. Chandrasekaran, M.D.P.S. Idelchik, J.A. Melendez, Redox control of senescence and age-related disease, Redox Biol. 11 (2017) 91–102.
[62] P. Davalli, et al., ROS, cell senescence, and novel molecular mechanisms in aging and age-related diseases, in: Oxidative Medicine and Cellular Longevity, 2016, 3565127.
[63] Z. Wang, D. Wei, H. Xiao, Methods of cellular senescence induction using oxidative stress, Methods Mol. Biol. 1048 (2013) 135–144.
[64] T. Armeni, et al., Cellular redox imbalance and changes of protein S-glutathionylation patterns are associated with senescence induced by oncogenic H-ras, PLoS One 7 (12) (2012), e52151.
[65] Y. Sun, et al., Glutathione depletion induces ferroptosis, autophagy, and premature cell senescence in retinal pigment epithelial cells, Cell Death Dis. 9 (7) (2018) 1–15.
[66] F. Yang, et al., Glutaredoxin-1 silencing induces cell senescence via p53/p21/p16 signaling axis, J. Proteome Res. 17 (3) (2018) 1091–1100.
[67] T.E. King, A. Pardo, M. Selman, Idiopathic pulmonary fibrosis, Lancet 378 (2011) 1949–1961.
[68] V.L. Kinnula, et al., Oxidative stress in pulmonary fibrosis: a possible role for redox modulatory therapy, Am. J. Respir. Crit. Care Med. 172 (2005) 417–422.
[69] S.C. Lu, Glutathione synthesis, Biochim. Biophys. Acta 1830 (5) (2013) 3143–3153.
[70] J.R. Terrill, et al., N-Acetylcysteine treatment of dystrophic mdx mice results in protein thiol modifications and inhibition of exercise induced myofibre necrosis, Neuromuscul. Disord. 22 (5) (2012) 427–434.
[71] G. Aldini, et al., N-Acetylcysteine as an antioxidant and disulphide breaking agent: the reasons why, Free Radic. Res. 52 (7) (2018) 751–762.
[72] A. Musaogullari, Y.C. Chai, Redox regulation by protein S-glutathionylation: from molecular mechanisms to implications in health and disease, Int. J. Mol. Sci. 21 (21) (2020) 8113.
[73] Y. Xiong, et al., S-glutathionylation: from molecular mechanisms to health outcomes, Antioxidants Redox Signal. 15 (1) (2011) 233–270.
[74] D. Crans, et al., The chemistry and biochemistry and the biological activities exerted by vanadium compounds, Chem. Rev. 104 (2004) 849–902.
[75] R.P. Szajewski, G.M. Whitesides, Rate constants and equilibrium constants for thiol-disulfide interchange reactions involving oxidized glutathione, J. Am. Chem. Soc. 102 (6) (1980) 2011–2026.

[76] A.M. Cortizo, et al., A possible role of oxidative stress in the vanadium-induced cytotoxicity in the MC3T3E1 osteoblast and UMR106 osteosarcoma cell lines, Toxicology 147 (2) (2000) 89–99.
[77] Z. Zhang, et al., Vanadate-induced cell growth regulation and the role of reactive oxygen species, Arch. Biochem. Biophys. 392 (2) (2001) 311–320.
[78] M.A.M. Capella, et al., *Vanadate-induced cell death is dissociated from H2O$_2$ generation*, Cell Biol. Toxicol. 23 (6) (2007) 413–420.
[79] N. Chatterjee, et al., *Diperoxovanadate can substitute for H_2O_2 at much lower concentration in inducing features of premature cellular senescence in mouse fibroblasts (NIH3T3)*, Mech. Ageing Dev. 132 (5) (2011) 230–239.
[80] L. Marti, et al., Tyramine and vanadate synergistically stimulate glucose transport in rat adipocytes by amine oxidase-dependent generation of hydrogen peroxide, J. Pharmacol. Exp. Therapeut. 285 (1) (1998) 342–349.
[81] S. Portillo-Ledesma, et al., Deconstructing the catalytic efficiency of peroxiredoxin-5 peroxidatic cysteine, Biochemistry 53 (2014) 6113–6125.
[82] N. Hogg, R.J. Singh, B. Kalyanaraman, The role of glutathione in the transport and catabolism of nitric oxide, FEBS (Fed. Eur. Biochem. Soc.) Lett. 382 (3) (1996) 223–228.
[83] B.J. Day, Antioxidants as potential therapeutics for lung fibrosis, Antioxidants Redox Signal. 10 (2008) 355–370.
[84] S.B. Chia, et al., Dysregulation of the glutaredoxin/S-glutathionylation redox axis in lung diseases, Am. J. Physiol. Cell Physiol. 318 (2020) C304–C327, https://doi.org/10.1152/ajpcell.00410.2019.
[85] S. Teramoto, et al., Superoxide anion formation and glutathione metabolism of blood in patients with idiopathic pulmonary fibrosis, Biochem. Mol. Med. 55 (1) (1995) 66–70.
[86] R.-M. Liu, K.A.G. Pravia, Oxidative stress and glutathione in TGF-β-mediated fibrogenesis, Free Radic. Biol. Med. 48 (1) (2010) 1.
[87] K. Aquilano, S. Baldelli, M.R. Ciriolo, Glutathione: new roles in redox signaling for an old antioxidant, Front. Pharmacol. 5 (2014) 196.
[88] P. Jones D, Redox potential of GSH/GSSG couple: assay and biological significance, Methods Enzymol. 348 (2002) 93–112.
[89] F.Q. Schafer, G.R. Buettner, Redox environment of the cell as viewed through the redox state of the glutathione disulfide/glutathione couple, Free Radic. Biol. Med. 30 (2001) 1191–1212.
[90] D.P. Jones, Redefining oxidative stress, Antioxidants Redox Signal. 8 (9-10) (2006) 1865–1879.
[91] A.M. Courtwright, S. El-Chemaly, Telomeres in interstitial lung disease: the short and the long of it, Ann. Am. Thorac. Soc. 16 (2) (2019) 175–181.
[92] I. Dalle-Donne, et al., S-glutathionylation in protein redox regulation, Free Radic. Biol. Med. 43 (6) (2007) 883–898.
[93] V. Anathy, et al., Reducing protein oxidation reverses lung fibrosis, Nat. Med. 24 (8) (2018) 1128–1135.
[94] S.W. Aesif, et al., in: In Situ Analysis of Protein S-Glutathionylation in Lung Tissue Using Glutaredoxin-1-Catalyzed Cysteine Derivatization, vol. 175, 2009, pp. 36–45, 1.